Molecular dynamics simulations of side chain liquid crystal polymer molecules in isotropic and liquid-crystalline melts

Lorna M. Stimson and Mark R. Wilson[a)]
Department of Chemistry, University of Durham, South Road, Durham, DH1 3LE, United Kingdom

(Received 4 March 2005; accepted 13 May 2005; published online 27 July 2005)

A detailed molecular dynamics simulation study is described for a polysiloxane side chain liquid crystal polymer (SCLCP). The simulations use a coarse-grained model composed of a combination of isotropic and anisotropic interaction sites. On cooling from a fully isotropic polymer melt, we see spontaneous microphase separation into polymer-rich and mesogen-rich regions. Upon application of a small aligning potential during cooling, the structures that form on microphase separation anneal to produce a smectic-A phase in which the polymer backbone is largely confined between the smectic layers. Several independent quenches from the melt are described that vary in the strength of the aligning potential and the degree of cooling. In each quench, defects were found where the backbone chains hop from one backbone-rich region to the next by tunneling through the mesogenic layers. As expected, the number of such defects is found to depend strongly on the rate of cooling. In the vicinity of such a defect, the smectic-A structure of the mesogen-rich layers is disrupted to give *nematiclike* ordering. Additionally, several extensive annealing runs of approximately 40 ns duration have been carried out at the point of microphase separation. During annealing the polymer backbone is seen to be slowly excluded from the mesogenic layers and lie perpendicular to the smectic-A director. These observations agree with previous assumptions about the structure of a SCLCP and with interpretations of x-ray diffraction and small angle neutron scattering data. The flexible alkyl spacers, which link the backbone to the mesogens, are found to form sublayers around the backbone layer. © *2005 American Institute of Physics*. [DOI: 10.1063/1.1948376]

I. INTRODUCTION

Liquid crystal polymers (LCPs) may be classified according to the location of mesogenic groups within the polymer structure.[1] Polymers with rigid mesogenic groups incorporated within the backbone are termed main chain liquid crystal polymers (MCLCPs). These were the first type of liquid crystal polymers to be synthesized and include a range of nematogenic and smectogenic polymers, which have been known for many years.[2] Most notably, MCLCPs have found uses in the production of high strength fibers. Side chain liquid crystal polymers (SCLCPs) are formed when mesogenic units are attached to the polymer backbone as pendant groups. Here the tendency for the backbone to adopt a random coil conformation competes with the mesogenic preference for orientational order. The use of a flexible spacer group, such as a short carbon chain, to link the mesogens to the backbone,[3] decouples the mesogens slightly from the backbone conformation; however, the backbone still exerts a significant influence on mesomorphism. Such systems usually include thermotropic mesogens, which may form smectic and nematic phases.[4] The structure of the pendant mesogenic groups, the nature of the polymer backbone, the molecular weight, the tacticity, and the length of the flexible spacer length all exert an influence on mesophase formation.

Over the years, there have been a number of experimental studies of SCLCPs, aimed at understanding the relationship between polymer structure and mesophase formation. At the simplest level, optical microscopy and differential scanning calorimetry (DSC) can be used to determine phase boundaries.[5] However, these provide no direct information about the polymers at a molecular level. X-ray diffraction,[6] neutron diffraction,[7,8] and small-angle neutron scattering[7–15] (SANS) from well-aligned samples can, in principle, provide molecular level information. For neutron studies, the use of partial deuteration is particularly helpful in providing structural information about the arrangement of different parts of the polymer in the bulk mesophase. For smectics, the results point to a strong anisotropy in the conformations of the polymer backbone,[10] with the perpendicular component of the backbone radius of gyration (i.e., perpendicular to the direction of the order which is usually imposed by an aligning field) being larger than the parallel component. In other words, the backbone tends to align parallel to the smectic layers. For nematics, the radius of gyration is also found to be anisotropic. However, the nature of the anisotropy tends to be influenced by the presence/absence of an underlying smectic phase, which can induce smectic fluctuations within the nematic. Many of the experiments in this area are technically demanding. Not least, are the difficulties in obtaining a good uniform alignment of the polymer, which sometimes demands high magnetic aligning fields of greater than 9 T.[10]

In contrast with the area of low molecular weight liquid crystals, where simulation has proved extremely successful at atomistic[16–20] and semiatomistic levels,[21–24] LCPs have

[a)]Author to whom correspondence should be addressed. Fax: +44 191 386 1127. Electronic mail: mark.wilson@durham.ac.uk

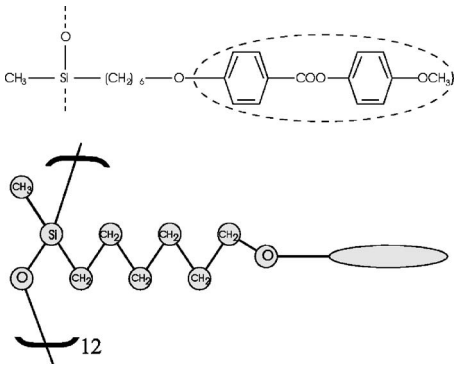

FIG. 1. Top: Chemical structure of a polymethylsiloxane SCLCP. Bottom: Schematic diagram of the model polymer used in this work.

proved difficult to study by simulation. Here the twin problems of large system sizes and long equilibration times have largely prevented simulations at an atomistic level, though some progress has been made at the semiatomistic level for MCLCPs.[25,26] Consequently, information about the molecular structure of SCLCPs within a mesophase is limited to that obtained from simple models which describe the x-ray and neutron results; and it has not been possible to produce simulations which examine the distribution of mesogenic groups, the position of flexible spacers, or the conformation of the backbone.

In the current study, we use a coarse-grained (CG) simulation model to provide, for the first time, a molecular picture of the order within a bulk mesophase formed by a SCLCP. The model polymer uses Lennard-Jones sites to represent the flexible siloxane backbone and the alkyl spacers, in combination with CG mesogenic moieties represented by Gay–Berne potentials. This hybrid model is described in detail in Sec. II. In Sec. III we present results looking at the behavior of the model as the system is cooled from an isotropic polymer melt with and without the application of an aligning potential. Results of extremely long annealing simulations are presented also. The simulations allow us to look at the ordering of the mesogenic units, the siloxane polymer backbone, and the flexible spacers within the bulk mesophases that form. Finally, we draw some conclusions in Sec. IV.

II. COMPUTATION

The simulations described in this study use a model SCLCP based on the structure given in Fig. 1. The polymer, which has been the subject of a number of experimental studies,[27,28] has a polydimethylsiloxane (PDMS) backbone, with a flexible spacer composed of a hexyl chain attached to each silicon atom. Mesogens are attached to the spacers via an oxygen atom. Figure 1 provides a schematic representation of the simulation model. The model used relies on a coarse-grained description for a flexible molecule, which has previously been adopted for the simulation of liquid crystal dimers,[29] a flexible mesogen with tails at both ends of the molecule[23] and a main chain liquid crystal polymer.[30] We use a degree of polymerization of $n=12$, and 64 separate polymer chains giving a total of 768 mesogenic groups. Four different types of site are used: representing silicon, oxygen atoms, carbon-united atoms, which are the same for the CH_2 as CH_3 groups, and an elliptical site representing the mesogenic unit. The silicon atoms in the backbone are four coordinate and so it is necessary to choose a stereochemistry for the arrangement of the pendant groups in the model system. Accordingly, we choose a syndiotactic arrangement of the side chains to minimize the steric repulsion between them.

The force field used to describe the model system takes the form

$$
\begin{aligned}
E_{\mathrm{Total}} = & \sum_{i=1}^{N_{\mathrm{angles}}} \frac{k_i^{\mathrm{ang}}}{2}(\theta_i - \theta_i^0)^2 + \sum_{i=1}^{N_{\mathrm{GB}}} k_i^{\mathrm{GBang}}(\upsilon_i - \upsilon_i^0)^2 \\
& + \sum_{i=1}^{N_{\mathrm{dihedrals}}} [a_{1,i}(1+\cos\phi_i) + a_{2,i}(1-\cos(2\phi_i)) \\
& + a_{3,i}(1+\cos(3\phi_i))] + \sum_{i=1}^{N_{\mathrm{LJ}}} \sum_{j>1}^{N_{\mathrm{LJ}}} U_{\mathrm{LJ}} \\
& + \sum_{i=1}^{N_{\mathrm{LJ}}} \sum_{j=1}^{N_{\mathrm{GB}}} U_{\mathrm{LJ/GB}} + \sum_{i=1}^{N_{\mathrm{GB}}} \sum_{j>i}^{N_{\mathrm{GB}}} U_{\mathrm{GB}} + U_{\mathrm{ext}}, \qquad (1)
\end{aligned}
$$

where N_{angles}, $N_{\mathrm{dihedrals}}$, N_{LJ}, and N_{GB} are the number of angles, the number of dihedral angles, the number of Lennard-Jones (LJ) sites, and the number of Gay–Berne (GB) sites, respectively, in the system. In Eq. (1) a harmonic potential is used to model bond angle deformations, where k_i^{ang} is a bond angle force constant, θ_i is the actual bond angle, and θ_i^0 is the equilibrium bond angle. The second term in Eq. (1) represents the angle between the orientation of a Gay–Berne site and the bond that connects it to the rest of the molecule: referred to as a GB-angle. The deformation of the GB-angle is modeled with a harmonic potential, with k_i^{GBang} as the angular force constant and υ_i and υ_i^0 as the actual and equilibrium GB-angles. The inclusion of the GB-angle term prevents free rotation of the mesogen about its center. The dihedral angle component of Eq. (1) is the third term, where ϕ_i is the dihedral angle and a_1, a_2, and a_3 are constants that parametrize the form of the potential for each type of dihedral angle. The terms U_{LJ}, $U_{\mathrm{LJ/GB}}$, and U_{GB} are the nonbonding interactions between each pair of sites. In this work, Lennard-Jones and Gay–Berne sites are used to represent spherical and elliptical sites, respectively, and the cross term $U_{\mathrm{LJ/GB}}$ is represented by a generalized potential for two unlike Gay–Berne particles. The expression for U_{LJ}, $U_{\mathrm{LJ/GB}}$, and U_{GB} are given in full in our previous work for low molecular weight flexible mesogens.[23] The final term in Eq. (1), U_{ext}, represents the interaction of the sites with an external magnetic field.

The force field parameters were obtained from previous hybrid GB/LJ studies of a liquid crystal dimer[31] and a mesogen with tails at both ends,[23] augmented by data from the MM2 force field for the siloxane part and updating the Ryckaert–Bellemans potential (used in Ref. 31) to the more recent work by Martin and Siepmann[32] and later Nath and Khare.[33] Bond lengths were constrained using the SHAKE procedure:[34] using bond lengths Si–O=1.626 Å, Si–C=1.880 Å, C–C=1.523 Å, C–O=1.402 Å, and

TABLE I. Force field parameters for atomic sites.

Atom	Mass/10^{-25} kg	ϵ/k_b/K	Source	σ/Å	Source
Si	0.466 296 5	72.0	43	3.932	23, 31, and 44
O	0.265 679 4	72.0	43	3.923	23, 31, and 44
CH_n	0.232 929 0	72.0	43	3.923	23, 31, and 44

O–GB=6.0 Å. The form of the Gay–Berne potential used has been studied in detail by de Miguel and co-workers[35–37] and the phase diagram is well known. It is characterized by the exponents $\mu=1$ and $\nu=2$; length-to-breadth ratio, $\sigma_{ee}/\sigma_{ss}=3$; and ratio of well depths, $\epsilon_{ee}/\epsilon_{ss}=1/5$. We define $\sigma_0^{GB}=\sigma_{ss}$ and $\epsilon_0^{GB}=\epsilon_{ss}$ throughout this work. The full potential is specified by parameters in Tables I–IV. Spherical nonbonded cutoffs were employed throughout for U_{LJ}, $U_{LJ/GB}$, and U_{GB} at 9.0, 16.5, and 18.8 Å, respectively. The GB and GB/LJ nonbonded potentials were shifted to ensure that the interactions went smoothly to zero. Long-range corrections to the energy and virial were evaluated for the LJ potential. Separate Verlet neighbor lists were used for each of the three nonbonded cutoffs. All 1-2, 1-3, or 1-4 terms were excluded from the nonbonded interactions in Eq. (1).

Molecular dynamics calculations were used to examine the phase behavior of the polymer. The simulations were carried out using the anisotropic form of the leapfrog algorithm[38] to solve the equations of motion, as implemented in the earlier work of one of the current authors on liquid crystal dimers.[29] The NpT ensemble was employed, at zero pressure with a 2 fs time step throughout the studies. A simple thermostat was implemented to allow the system to collide with a heat bath every 100 steps in order to maintain a constant temperature. The simulation box dimensions were allowed to vary using Monte Carlo moves, as described in the earlier dimer study.[29]

An array of 64 identical polymer molecules were placed in a simulation box and preliminary simulations were undertaken to relax the polymer configurations. These simulations were conducted at 600 K to ensure that the polymer was able to move freely and form a melt.

Preliminary investigations suggested that the system was extremely viscous and accordingly the annealing process was very slow. Therefore, it was envisaged that, as in real siloxane polymers, liquid crystal monodomains would only be obtained on cooling in the presence of an external electric or magnetic field. Consequently, an external potential was applied for some of the runs to mimic an external magnetic field. This torque on a mesogen in a magnetic field arises from the diamagnetic anisotropy of the mesogen. For most calamitic liquid crystals the magnitude of the diamagnetic susceptibility is larger perpendicular to the long molecular axis, rather than parallel to it, leading to a positive value for the anisotropy in magnetic susceptibility $\Delta\chi$ (i.e., $\chi_\parallel$ and $\chi_\perp$ are $-ve$ but $\Delta\chi=+ve$), which causes the liquid crystal to align parallel to the magnetic field. Accordingly, we adopt a simple form for the external potential

$$U_{\text{ext}}=\sum_{i=1}^{N_{\text{GB}}}-\epsilon^{\text{field}}\hat{\mathbf{u}}_{zi}^2, \tag{2}$$

favoring orientations parallel or antiparallel to the applied field (z axis), where $\hat{\mathbf{u}}_z$ is the z component of the Gay–Berne orientational vector.

Luckhurst and Saielli[39] have examined Gay–Berne mesogens in an external potential of this form. For high values of the strength parameter, ϵ^{field}, they find that smectic phases can be induced from a nematic. In their work, values for ϵ^{field} of $0.5\epsilon_0^{GB}$, $5.0\epsilon_0^{GB}$, and $8.0\epsilon_0^{GB}$ were used and phase transitions to the smectic were observed for the two larger field strengths, while the system with $\epsilon^{\text{field}}=0.5$ remained nematic. However, in the current study we were anxious not to apply an external potential of sufficient magnitude to induce shifts in the phase boundaries. Consequently, two trial potentials,

TABLE II. Force field parameters for Gay–Berne sites.

Parameter	Value	Source
Mass (GB)	$2.955\,796\,8\times10^{-25}$ kg	23 and 31
Inertia (GB)	$0.273\,05\times10^{-23}$ kg Å^2	23 and 31
$\epsilon_0^{GB}/k_b=\epsilon_{ee}/k_b$	406.51 K	23 and 31
$\epsilon_0^{GB/LJ}/k_b$	171.08 K	23 and 31
$\sigma_0^{GB}=\sigma_{ss}$	4.721 Å	23 and 31
$\sigma_0^{GB/LJ}$	4.117 Å	23 and 31
v_i^0	0.0	21
$k_i^{GB_{ang}}/k_B$	62 680 K	32 and 33
$\chi\alpha^{-2}$	0.552 79	23 and 45
$\chi'\alpha'^{-2}$	0.770 27	23 and 45

TABLE III. Bond angle parameters.

Bond angle	Eq. angle θ^0/°	Source	Force constant (k^{ang}/k_B)/K rad^{-2}	Source
Si–O–Si	145.7		62 500	32 and 33
O–Si–O	113.5	46	32 580	46
O–Si–C	108.5	46	25 340	46
Si–C–C	109.0	46	28 960	46
C–Si–C	110.8	46	34 750	46
C–C–C	114.0	32 and 33	62 500	32 and 33
C–C–O	107.5	46	50 680	46
C–O–GB	115.8	AM1 calculation	62 500	32 and 33

TABLE IV. Dihedral angle parameters.

Dihedral Angle ϕ	Force constants/K a_1	a_2	a_3	Source
Si–O–Si–O	0.0	0.0	0.0	-
	0.0	0.0	503.23	-
O–Si–C–C	0.0	0.0	84.03	46
C–Si–C–C	0.0	150.97	84.03	46
Si–C–C–C	355.04	−68.19	791.32	C–C–C–C from Refs. 32 and 33
C–C–C–C	355.04	−68.19	791.32	C–C–C–C from Refs. 32 and 33
C–C–C–O	355.04	−68.19	791.32	C–C–C–C from Refs. 32 and 33
C–C–O–GB	355.04	−68.19	791.32	C–C–C–C from Refs. 32 and 33

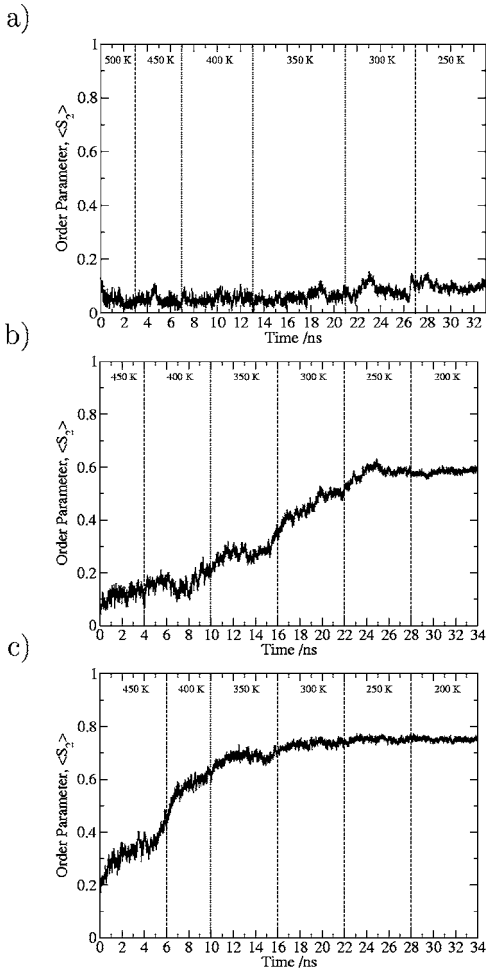

FIG. 2. Order parameter on slow cooling from an equilibrated isotropic melt at 500 K, using an aligning potential with (a) $\epsilon^{\text{field}}=0.0\times10^{-20}$ J, (b) $\epsilon^{\text{field}}=0.2\times10^{-20}$ J, and (c) $\epsilon^{\text{field}}=0.5\times10^{-20}$ J.

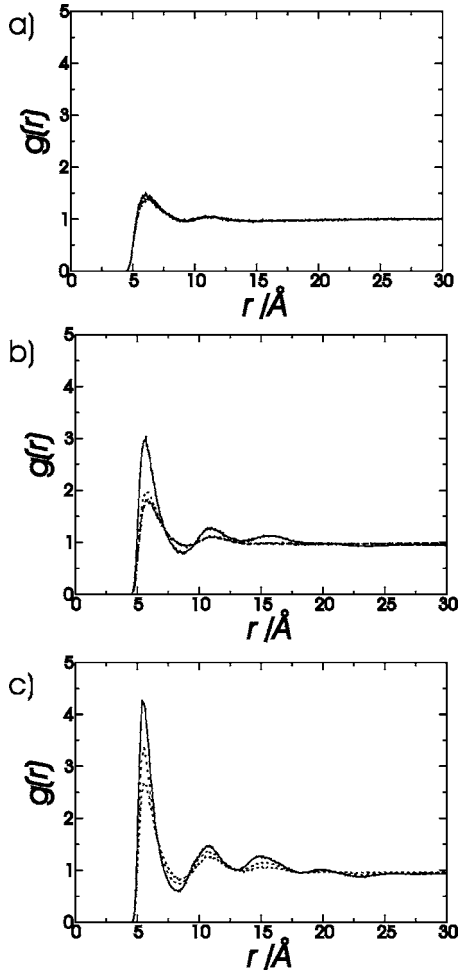

FIG. 3. Radial distribution functions, $g(r)$, for configurations at (a) 450 K, (b) 350 K, and (c) 250 K. Bold line - $\epsilon^{\text{field}}=0.5\times10^{-20}$ J, dotted line - $\epsilon^{\text{field}}=0.2\times10^{-20}$ J, and dashed line - $\epsilon^{\text{field}}=0.0\times10^{-20}$ J.

$\epsilon^{\text{field}}=0.36\epsilon_0^{\text{GB}}$ and $0.89\epsilon_0^{\text{GB}}$, respectively, 0.2×10^{-20} and 0.5×10^{-20} J, were employed only after initial testing on a known system.

A test system consisting of 256 Gay–Berne sites was initially prepared to test the aligning potential. Each Gay–Berne site was parametrized to match the ones in the SCLCP. The test simulations were conducted at 400 K, with a 10-fs time step and a cut-off radius of 18.88 Å. Initially, we equilibrated the test system at a state point in the nematic region of the phase diagram and measured the equilibrium value of $\langle S_2\rangle$. We then applied the aligning potential perpendicular to the liquid crystal director and measured the time taken for realignment of the nematic and noted the equilibrium order parameter for the realigned phase. Here, we found that values of 0.5×10^{-20} and 0.2×10^{-20} J for ϵ^{field} were sufficient to align a nematic in 350 and 1000 ps, respectively. In the case of the former, the equilibrium order parameter, $\langle S_2\rangle$, was unchanged relative to the original equilibrium nematic with no field applied. For the latter, $\langle S_2\rangle$ changed by less than 0.05. We note, in passing, that a value of ϵ^{field} of 1.0×10^{-20} J is able to rapidly realign the director within 250 ps but causes an increase in the nematic order parameter of approximately 0.15.

III. RESULTS AND DISCUSSION

A. Phase behavior on cooling from isotropic melt

To observe the phase behavior of the model system, a sample was cooled slowly from an equilibrated isotropic melt at 500 K over a period of 35 ns with no external potential applied. A further two sets of molecular dynamics (MD) runs were started from the same isotropic configuration, employing ϵ^{field} values of 0.2×10^{-20} and 0.5×10^{-20} J, respectively. The configurations of the system at each temperature were analyzed by computing order parameters, radial distribution functions, and diffusion constants.

The ensemble-averaged Gay–Berne order parameter is given by

$$\langle S_2\rangle = \langle P_2(\cos\theta)\rangle, \tag{3}$$

where θ is the angle of the Gay–Berne axis relative to the uniaxial director of the system. $\langle S_2\rangle$ is shown for the three cooling runs in Fig. 2. In the absence of an external potential [Fig. 2(a)] the average overall order in the system does not change significantly with cooling. However, application of the small aligning potential, with $\epsilon^{\text{field}}=0.2\times10^{-20}$ J, is sufficient to induce a large change in the order parameter during the cooling run [Fig. 2(b)], with growth in orientational order

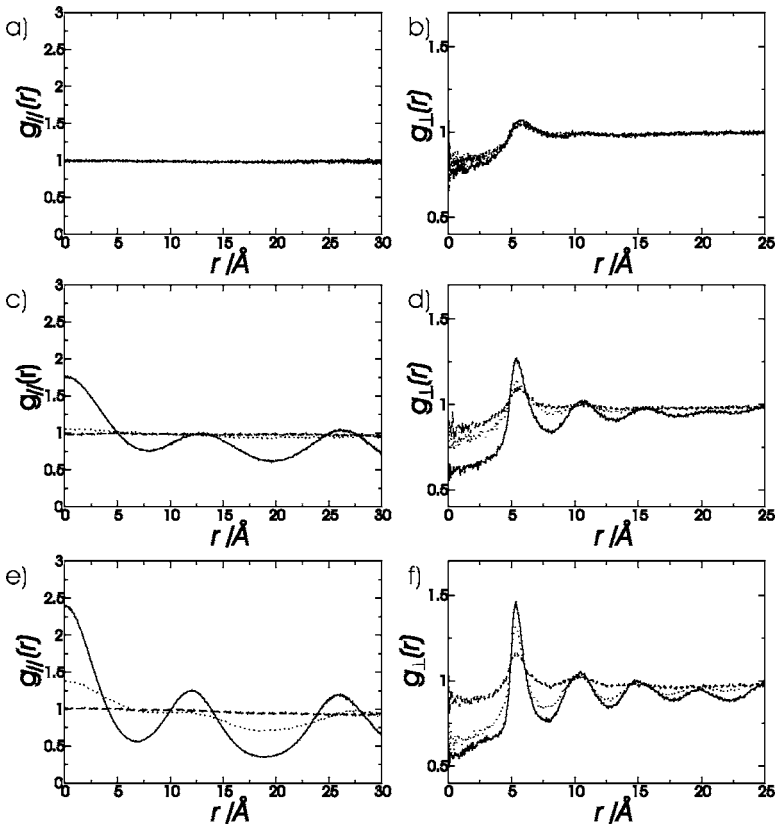

FIG. 4. Components of the radial distribution function parallel and perpendicular to the director (a) $g_{\parallel}(r)$ at 450 K, (b) $g_{\perp}(r)$ at 450 K, (c) $g_{\parallel}(r)$ at 350 K, (d) $g_{\perp}(r)$ at 350 K, (e) $g_{\parallel}(r)$ at 250 K, and (f) $g_{\perp}(r)$ at 250 K. Bold line - $\epsilon^{\text{field}}=0.5\times10^{-20}$ J, dotted line - $\epsilon^{\text{field}}=0.2\times10^{-20}$ J, and dashed line - $\epsilon^{\text{field}}=0.0\times10^{-20}$ J.

occurring over a 15 ns time scale in cooling from 400 to 250 K and $\langle S_2\rangle$ reaching an approximate value of 0.6 at 250 K. On cooling with the higher value of ϵ^{field} [Fig. 2(c)], a rapid increase in the order parameter is observed and the sample becomes well ordered with $\langle S_2\rangle$ reaching a final value of 0.75 at 300 K. After which there is no change in orientational ordering on further cooling. From the results of our earlier test simulations on the Gay–Berne mesogen (Sec. II), the aligning potentials are predicted to be too weak to induce a phase transition or influence the value of $\langle S_2\rangle$ in a homogeneous liquid crystal. However, the potentials should be sufficiently large to influence the distribution of the local director in separate liquid-crystalline domains; thereby influencing $\langle S_2\rangle$ for the system as a whole. This is discussed further below.

To understand better the structure of the polymer during the cooling process, radial distribution functions were calculated for Gay–Berne sites using the final 1 ns of data for each temperature. Results are shown for the radial distribution function $g(r)$ (Fig. 3) and its components perpendicular, $g_{\perp}(r)$, and parallel, $g_{\parallel}(r)$, to the director (Fig. 4) and the pairwise orientational distribution function, $g_2(r)$ (Fig. 5), for three sample temperatures at 450, 350, and 250 K.

At 450 K, $g(r)$ curves in Fig. 3(a) show typical liquidlike structure, and are identical for each aligning potential. The nearest-neighbor peak is close to 5.3 Å, the minimum in the potential for side-to-side interactions. The second nearest-neighbor peak is very weak, smaller than in most liquids, indicating no clustering of Gay–Berne particles at this temperature. In addition, the lack of structure in $g_{\parallel}(r)$ [Fig. 4(a)] confirms that there are no layers or domains forming at this temperature. In Fig. 5(a), $g_2(r)$ at 450 K shows some alignment of nearest neighbors in the first solvation shell. The value of $g_2(r)$ at long distances tends to $\langle S_2\rangle^2$ and we note that a very small degree of field-induced long-range order is evident for the largest aligning potential. This is typical of that seen in the isotropic pretransitional region of real mesogens under the application of a strong electric field (the Kerr effect).[40] However, the lower of value of ϵ^{field} is insufficient to produce any noticeable change in $g_2(r)$ compared to the zero-field case.

At 350 K, the ordering potential induces clear changes in the polymer structure. For the highest value of ϵ^{field}, $g(r)$ [Fig. 3(b)] the nearest-neighbor peak grows and two other peaks are also evident at approximately two and three times the separation distance of the nearest-neighbor peak. In Figs. 4(c) and 4(d), peaks and troughs appear in $g_{\parallel}(r)$, which are indicative of smectic layers and a typical dense liquidlike signature is seen in $g_{\perp}(r)$, indicating that the smectic formed is a fluid, i.e., smectic A or smectic C. No layer ordering is seen for $\epsilon^{\text{field}}=0.2\times10^{-20}$ J at this temperature, though a small degree of long-range order is seen in $g_2(r)$ [Fig. 5(b)] suggesting that the system is close to the phase transition to a liquid crystal.

At 250 K the radial distributions indicate that the two samples cooled in a field are both in a smectic-A phase. All three systems show three solvation shell peaks [Fig. 3(c)], there is also a possible fourth peak in the distribution for the sample in the $\epsilon^{\text{field}}=0.5\times10^{-20}$ J sample. In Fig. 5(c), $g_2(r)$ shows an increase in orientational order for the systems with an external potential applied and the peaks indicate strong orientational correlation out to the third nearest neighbor in each case. The presence of layers is shown in $g_{\parallel}(r)$ [Fig. 4(c)] for the two systems in the aligning field. Here, it is

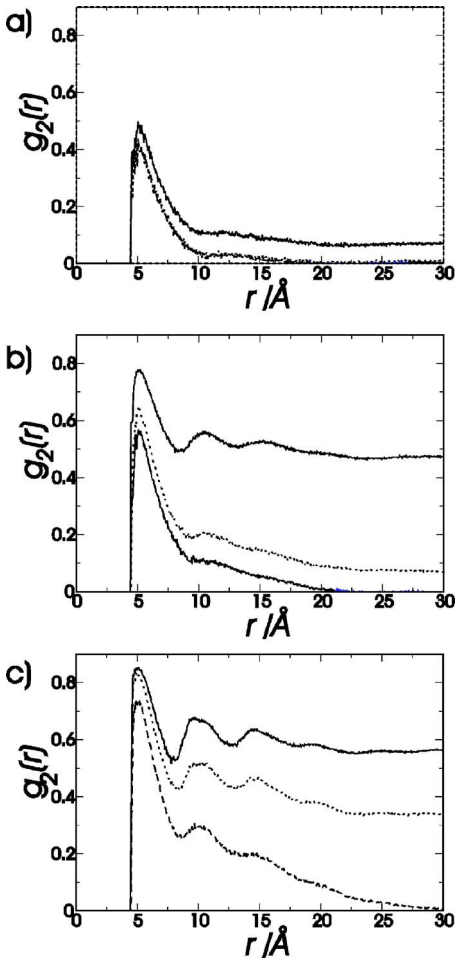

FIG. 5. Pairwise orientational correlation function, $g_2(r)$ for equilibrated configurations at (a) 450 K, (b) 350 K, and (c) 250 K. Bold line - $\epsilon^{\text{field}}=0.5\times10^{-20}$ J, dotted line - $\epsilon^{\text{field}}=0.2\times10^{-20}$ J, and dashed line - $\epsilon^{\text{field}}=0.0\times10^{-20}$ J.

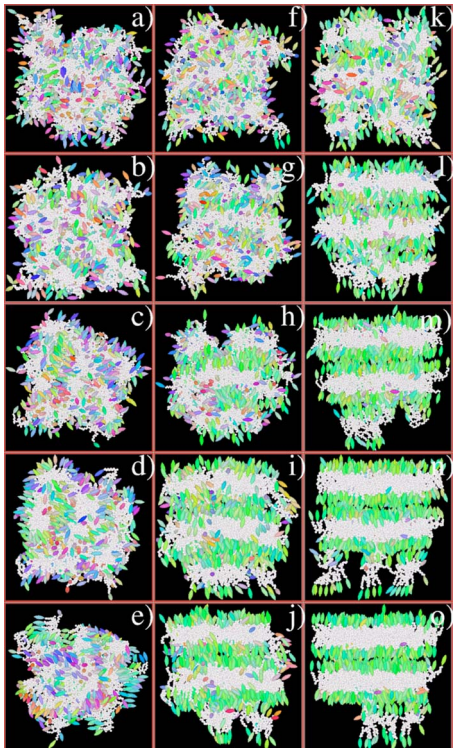

FIG. 6. Snapshots of system configurations for a series of state points. Column 1 - a–e, $\epsilon^{\text{field}}=0.0\times10^{-20}$ J. Column 2 - f–j, $\epsilon^{\text{field}}=0.2\times10^{-20}$ J. Column 3 - k–o, $\epsilon^{\text{field}}=0.5\times10^{-20}$ J. Row 1 - *a,f,k* at 450 K. Row 2 - *b,g,l* at 400 K. Row 3 - *c,h,m* at 350 K. Row 4 - *d,i,n* at 300 K. Row 5 - *e,j,o* at 250 K.

clear that the magnitude of the external potential has a pronounced influence on the formation of well-defined layers (see Sec. III B). Figure 4(f) shows the perpendicular component of the radial distribution function at 250 K, which should show up any order within smectic layers. In the absence of the aligning potential there is little structure but for the samples in the external potential there are a number of peaks. As before, the liquidlike signature here suggests that the smectic phase formed has no long-range in-layer ordering and is therefore a fluid smectic.

Configurations of the system were extracted from the three cooling runs at a range of temperatures and a sample are shown in Fig. 6. At high temperatures, in the absence of an applied external potential, full mixing occurs between the polymeric parts of the molecule and the mesogens. When this sample is cooled some microphase separation is evident from the formation of mesogen- and polymer-rich regions and the color coding in Fig. 6 indicates that alignment of Gay–Berne particles occurs within mesogenic domains. However, the local nematic director is effectively uncoupled within each domain. This explains the growth in the value of $g_2(r)$ for short distances [Fig. 5(c)] but the absence of any long-range order.

The effect of the smaller aligning potential is seen in column 2 of Fig. 6, where the system goes from complete mixing of mesogen and polymer at 450 K, to the start of microphase separation at 350 K. Here, however, in contrast with the $\epsilon^{\text{field}}=0.0\times10^{-20}$ J simulation, microphase separation leads to domains forming with the local domain director pointing in a common direction. This in turn encourages layer formation and well-defined smectic layers form as the system is cooled further.

Finally, column 3 of Fig. 6 shows the system with an external potential of field strength 0.5×10^{-20} J applied. With this stronger field the system phase separates much sooner and layers can be seen even at 400 K. However, the order within these layers appears nematiclike. When the sample is cooled to 350 K the strata become well developed and a pattern with one polymer layer sandwiched between two mesogen layers emerges. The ordering inside the mesogenic layers seems quite fluid at this stage. At 250 K the 2:1 morphology sharpens and smectic-A order within the mesogen layers is observed, explaining the peaks in $g_\perp(r)$ in Fig. 4(f).

For the higher value of ϵ^{field}, we have examined the behavior of the system, when the field is removed. Here, it seems clear that once formed, the lamellar morphology is stable over long time periods. For example, long annealing runs have been carried out at 300 and 350 K for 28 and 34 ns, respectively. In both cases, the additional, nonintrinsic order caused by the aligning potential is rapidly lost with a drop in $\langle S_2\rangle$ to approximately 0.62 occurring within the first 0.5 ns of simulation time. However, the system then remains unchanged over the remainder of the run, with just the nor-

TABLE V. Diffusion coefficients calculated over the last 2 ns of the simulation. For the Gay–Berne sites (GB), a Lennard-Jones site at the end of the polymer backbone (LJ_1), and a Lennard-Jones site in the middle of the polymer backbone (LJ_2).

Temp. /K	ϵ^{field} $/\times 10^{-20}$ J	D(GB) $/m^2\,s^{-1}$	$D(LJ_1)$ $/m^2\,s^{-1}$	$D(LJ_2)$ $/m^2\,s^{-1}$
500	0.0	$2.39\pm0.36\times10^{-10}$	$1.10\pm0.13\times10^{-10}$	$7.06\pm0.40\times10^{-11}$
450	0.0	$1.50\pm0.11\times10^{-10}$	$6.92\pm0.93\times10^{-11}$	$4.40\pm0.55\times10^{-11}$
400	0.0	$8.54\pm2.05\times10^{-11}$	$4.75\pm0.86\times10^{-11}$	$2.66\pm0.31\times10^{-11}$
350	0.0	$5.12\pm1.25\times10^{-11}$	$2.79\pm0.76\times10^{-11}$	$1.54\pm0.36\times10^{-11}$
300	0.0	$2.22\pm0.61\times10^{-11}$	$1.56\pm0.42\times10^{-11}$	$6.60\pm0.98\times10^{-12}$
250	0.0	$8.08\pm3.36\times10^{-12}$	$4.55\pm0.85\times10^{-12}$	$1.88\pm0.34\times10^{-12}$
450	0.2	$1.17\pm0.27\times10^{-10}$	$6.95\pm1.02\times10^{-11}$	$4.36\pm0.26\times10^{-11}$
400	0.2	$7.83\pm1.03\times10^{-11}$	$4.96\pm1.69\times10^{-11}$	$3.01\pm0.96\times10^{-11}$
350	0.2	$5.23\pm0.22\times10^{-11}$	$2.06\pm0.58\times10^{-11}$	$1.33\pm0.50\times10^{-11}$
300	0.2	$2.27\pm0.18\times10^{-11}$	$1.06\pm0.31\times10^{-11}$	$4.39\pm0.07\times10^{-12}$
250	0.2	$9.19\pm0.76\times10^{-12}$	$3.23\pm0.61\times10^{-12}$	$1.26\pm0.26\times10^{-12}$
200	0.2	$1.87\pm0.70\times10^{-12}$	$1.05\pm0.31\times10^{-12}$	$3.30\pm0.22\times10^{-13}$
450	0.5	$8.45\pm1.88\times10^{-11}$	$6.34\pm0.49\times10^{-11}$	$4.18\pm0.47\times10^{-11}$
400	0.5	$4.41\pm1.08\times10^{-11}$	$2.77\pm1.50\times10^{-11}$	$1.50\pm0.49\times10^{-11}$
350	0.5	$2.62\pm0.82\times10^{-11}$	$1.55\pm0.12\times10^{-11}$	$5.75\pm2.89\times10^{-12}$
300	0.5	$8.76\pm2.70\times10^{-12}$	$5.48\pm2.12\times10^{-12}$	$2.22\pm0.27\times10^{-12}$
250	0.5	$4.08\pm2.71\times10^{-12}$	$1.38\pm0.51\times10^{-12}$	$8.12\pm5.36\times10^{-13}$
200	0.5	$1.58\pm1.03\times10^{-12}$	$9.39\pm3.76\times10^{-13}$	$3.30\pm3.01\times10^{-13}$

mal small fluctuations in order parameter about a steady mean, which would be expected in a low molecular weight liquid crystal.

Approximate diffusion coefficients, D, have been obtained from the limiting slope of the mean square displacement (MSD) at long times using

$$D = \frac{1}{6t}\lim_{t\to\infty}|\langle|\mathbf{r}_i(t_2) - \mathbf{r}_i(t_1)|^2\rangle, \tag{4}$$

where $\mathbf{r}_i(t_1)$ and $\mathbf{r}_i(t_2)$ are the molecular position vectors at times t_1 and t_2, respectively, and the angular brackets denote an average over all molecules and a series of independent time origins. Diffusion coefficients have been calculated for three groups of sites in the molecule: all the Gay–Berne sites, the Lennard-Jones atom at the center of each polymer backbone, and a Lennard-Jones atom at the end of each backbone chain, in each case using the limiting slopes over the final 2 ns at each temperature, shown in Table V. The data confirm that the systems remain fluid down to 250 K and certainly at the point where microphase separation and growth of layers occur at 350 K. As we would expect, motion is highest for the mesogenic groups and smallest for the midchain atoms. It is interesting to compare the values here with those extracted from atomistic studies of low molecular weight liquid crystals in nematic phases. Usually, the latter are found to be ca. 10^{-10} $m^2\,s^{-1}$,[41] that is 10–100 times higher than those found for the polymer studied here. The viscosity of the polymer and the smectic nature of the mesophase dramatically slow the movement of sites. Plots of $\log D$ as a function of temperature are shown in Fig. 7. We note no large change in slope on cooling, as might be expected with a glass transition. (Though observation of this would be unlikely for the relatively short polymers studied here and the relatively quick rate of cooling employed.) However, in each case we see a small change in the slope of the $\log D$ between 300 and 350 K, associated with microphase separation. This occurs for both the polymer chain and the mesogens.

B. Influence of long-time annealing and faster cooling

Two state points were chosen for further investigation. For the $\epsilon^{field}=0.0\times10^{-20}$ J and $\epsilon^{field}=0.2\times10^{-20}$ J cases, long annealing runs (38 ns) were carried out at a fixed temperature of 350 K, starting from the 350 K end points of the runs shown in Fig. 2, i.e., the point where microphase separation starts to occur. In the presence of the smaller aligning potential, the order parameter grows over a period of 13 ns from a value of approximately 0.38–0.6, reaching a steady value of 0.62 over the course of the full 38 ns. Evidence from snapshots and distribution functions show that the same lamellar structure is formed as that obtained from the earlier cooling run with the high value of ϵ^{field} after annealing in the absence of an applied potential. The order parameter here is also identical to that obtained in the earlier simulation.

Without the aligning potential we were unable to fully anneal the structure to give well-formed lamellar layers, though we do get a small growth in $\langle S_2\rangle$ to a value of 0.2 over the course of 38 ns. Extensive analysis of snapshots from this run shows the slow growth of at least two substantial liquid-crystalline domains with the local director of each domain pointing in different directions. These are separated by polymer-rich regions in which the polymer has started to segregate to form layers. The difficulty here in obtaining uniform layers without a field is not altogether surprising and it is worth noting that in many experimental studies of LCPs, the high viscosity means that a strong external field (often in the region of 9 T or above for a magnetic field) must be applied to obtain good alignment. Characteristic textures of thin films of LCPs observed using polarizing microscopy often take days or weeks to anneal. It is unlikely that such

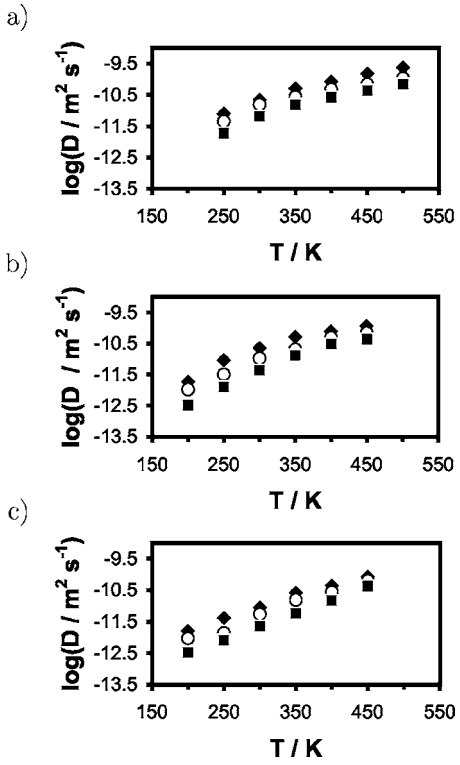

FIG. 7. $\log_{10} D$ plotted as a function of temperature for (a) $\epsilon^{\text{field}}=0.0\times10^{-20}$ J, (b) $\epsilon^{\text{field}}=0.2\times10^{-20}$ J, and (c) $\epsilon^{\text{field}}=0.5\times10^{-20}$ J. (Filled diamonds: Gay–Berne mesogens. Open circles: end atom of backbone. Filled squares: midatom of backbone.)

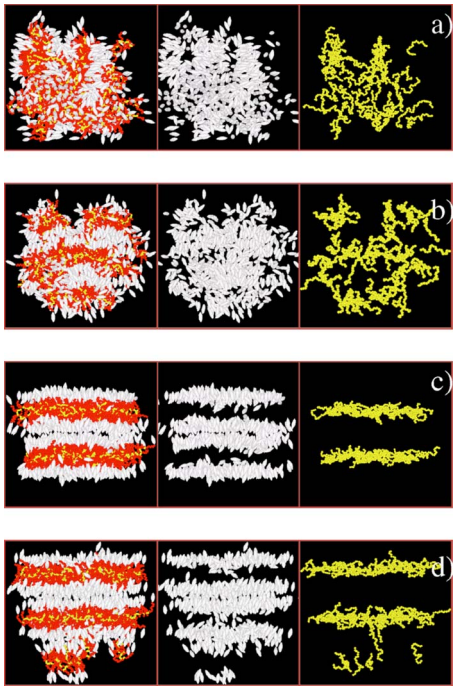

FIG. 8. Snapshots showing separate parts of the polymer molecules. (a) $\epsilon^{\text{field}}=0.0\times10^{-20}$ J after 38-ns annealing run at 350 K. (b) $\epsilon^{\text{field}}=0.2\times10^{-20}$ J from the original cooling run after 6 ns at 350 K. (c) $\epsilon^{\text{field}}=0.2\times10^{-20}$ J after further 38 ns of annealing at 350 K. (d) $\epsilon^{\text{field}}=0.5\times10^{-20}$ J from the original cooling run after 6 ns at 350 K. Left-hand column shows the full polymer, the middle columns shows only the mesogenic units and the right-hand column shows the backbone only. Shading: dark gray, polymer backbone, white, mesogenic units, and light gray, flexible spacer.

long times would be required in a simulation, as the length scales used in simulation are several orders of magnitude shorter than the structures seen in characteristic microscopy textures. However, time scales of several milliseconds may still be needed. The 40 ns simulations described here represent extremely long MD runs for a 2 fs time step. Currently, the only hope for studying the development of bulk structure in SCLCPs over longer length scales comes from dissipative particle dynamics (DPD)-type soft particle models, which can use longer time steps and which have shorter correlation times. Of particular note in this context is the recent work on rod-coil diblock copolymers by Al Sunaidi *et al.*,[42] which could easily be extended to SCLCP systems.

For the $\epsilon^{\text{field}}=0.5\times10^{-20}$ J model, we have carried out a more rapid cooling run starting from the isotropic melt at 500 K and cooling by 50 K every 2 ns down to a temperature of 200 K. Here, we obtained a linear increase in $\langle S_2\rangle$ up to a value of approximately 0.7 at the end of the 300 K run; and no change thereafter. Observation of snapshots and distribution functions from this independent quench show the same lamellar smectic-A structure obtained previously. However, in this case, the layers have more defects caused by one or more polymer backbones bridging between layers (see below). This is responsible for the small reduction in order parameter by about 0.03–0.04 in comparison with the previous slower cooling run in the same field.

C. Structure of the polymer in the smectic-A phase

The polymer morphology for each system can be examined by looking separately at regions occupied by different parts of the SCLCP molecules. In Fig. 8 this is done for state points at 350 K using the data from the cooling run with $\epsilon^{\text{field}}=0.2\times10^{-20}$ J [Fig. 8(b)] and $\epsilon^{\text{field}}=0.5\times10^{-20}$ J [Fig. 8(d)], and the two long annealing runs described in Sec. III B [Figs. 8(a) and 8(c)]. Figure 8(a) confirms the presence of microphase separation in the absence of a field, showing the presence of large liquid crystal regimes with local directors pointing in different directions. Also shown are the first signs of the formation of a lamellar layer in part of the simulation box.

It is interesting to compare the snapshots from the $\epsilon^{\text{field}}=0.2\times10^{-20}$ J results in Figs. 8(b) and 8(c). With the field applied, lamellar layers are able to form at the same point as microphase separation starts to occur. At this stage the polymer backbone straddles different mesogenic layers and this prevents the rapid annealing into well-defined layers that one would expect in a low molecular weight system. Indeed for the additional quench run, where temperature was dropped by 50 K every 2 ns, this type of structure initially forms and is "frozen in" at 200 K where further motion become very sluggish. However, in annealing at 350 K over 38 ns, the polymer backbone is gradually expelled completely from the mesogen-rich areas. As a result of this, in Fig. 8(b), the Gay–Berne mesogens, which remained nematic in Fig. 8(a), form a smectic-A structure with two clear layers of mesogens and the backbone is confined to a region about the width of a single smectic layer. The system size available in this study is, of course, rather limited by computer time. Consequently the width of the smectic layers is probably

influenced strongly by the system size employed. However, the surprising result for the backbone is entirely consistent with earlier x-ray-diffraction, neutron-diffraction, and small-angle neutron-scattering (SANS) results, described in Sec. I.

The second interesting observation from the layer structures in Fig. 8(c) is that the flexible spacers in this study become confined to the layers also, forming a sandwich either side of the polymer backbone. This has not been predicted previously and is certainly a result of the strong affinity that Gay–Berne particles have for each other, which drives the segregation of Gay–Berne and Lennard-Jones sites as temperature is lowered.

The "burrowing" of the backbone between polymer-rich layers is seen in the right-hand side of Fig. 8(d) for the well-ordered lamellar structure found in the high-field cooling run. The backbone is always associated with attached spacers, so burrowing therefore causes a sizable defect in the liquid-crystalline layer. In terms of mesogenic ordering, a defect manifests itself by the formation of a region of nematic ordering within a layer which would otherwise show pure smectic-A ordering of the mesogens. For long chains, one might expect that such defects must always occur, as configurational entropy will provide a larger driving force opposing confinement of single chains to individual layers. However, SANS studies by Richardson *et al.*[10] indicate the surprising result that the confinement of the backbone seems to increase with increasing molecular weight. The conclusion to this would be that chain ends are the important factor in facilitating the hopping of the backbone between layers. It would be interesting to test this by further simulation of longer chains.

IV. CONCLUSIONS

The work described in this study represents a detailed look at the phase behavior of a model polysiloxane SCLCP using a hybrid Gay–Berne/Lennard-Jones model. On cooling from a fully isotropic polymer, we see spontaneous microphase separation into polymer- and mesogen-rich regions. Under the application of a small aligning potential, applied during cooling, the structures formed on microphase separation anneal to produce a smectic-A structure in which the polymer backbone is largely confined between the liquid crystal layers. Several independent quenches have been carried out varying the strength of the applied aligning potential and the degree of cooling. Each give the same smectic structure, which is stable upon removal of the field and appears to be the equilibrium structure for the model polymer. Extensive annealing in the absence of a field gives liquid-crystalline domains but the time scale required to form a uniform lamellar structure is too long to observe with molecular dynamics.

In the well-aligned smectic phases, the backbone is found to be perpendicular to the smectic-A director in agreement with previous assumptions about the structure of SCLCPs and in agreement with the interpretations from earlier experimental work.[8–11] The flexible spacers are found to form sublayers around a "backbone" layer. For some quenches, defects were found where backbone chains span two layers. As expected, the number of such defects is found to depend strongly on the rate of cooling. In the vicinity of the defects, the smectic-A structure of the mesogen-rich layers is disrupted to give nematiclike ordering.

ACKNOWLEDGMENTS

The authors wish to thank Professor Rob Richardson (University of Bristol) for valuable discussions; the UK research council, EPSRC, for providing computer time and a studentship for one of the authors (L.M.S.) (1999–2002).

[1] H. Ringsdorf and A. Schneller, Br. Polym. J. **13**, 43 (1981).
[2] R. Centore and P. Inaelli, in *Liquid Crystal Polymers*, edited by C. Carfagna (Elsevier, New York, 1994), Chap. 3, pp. 31–45.
[3] H. Finkelmann, H. Ringsdorf, and J. Wendorff, Makromol. Chem. **179**, 273 (1978).
[4] H.-G. Noh, H.-K. Shim, J.-H. Chang, and J.-I. Jin, Macromolecules **30**, 1521 (1997).
[5] R. J. Sarna, G. P. Simon, G. Day, H.-J. Kim, and W. R. Jackson, Macromolecules **27**, 1603 (1994).
[6] P. Davidson and A. Levelut, Liq. Cryst. **11**, 469 (1992).
[7] L. Noirez, Europhys. Lett. **46**, 728 (1999).
[8] S. Lecommandoux, L. Noirez, M. Achard, and F. Hardouin, Macromolecules **33**, 67 (2000).
[9] I. Hamley, J. Fairclough, S. King, J. Pedersen, R. Richardson, C. Imrie, and A. Craig, Liq. Cryst. **22**, 679 (1997).
[10] R. M. Richardson, E. B. Barmatov, I. J. Whitehouse, V. P. Shibaev, T. Yongjie, and M. H. F. Godhino, Mol. Cryst. Liq. Cryst. Sci. Technol., Sect. A **330**, 285 (1999).
[11] S. Lecommandoux, L. Noirez, M. Achard, and F. Hardouin, J. Phys. II **7**, 1417 (1997).
[12] S. Picken, L. Noirez, and G. Luckhurst, J. Chem. Phys. **109**, 7612 (1998).
[13] P. Davidson, L. Noirez, J. Cotton, and P. Keller, Liq. Cryst. **10**, 111 (1991).
[14] L. Noirez, P. Keller, and J. Cotton, Liq. Cryst. **18**, 129 (1995).
[15] S. Lecommandoux, L. Noirez, H. Richard, M. Achard, C. Strazielle, and F. Hardouin, J. Phys. II **6**, 225 (1996).
[16] R. Berardi, L. Muccioli, and C. Zannoni, ChemPhysChem **5**, 104 (2004).
[17] M. R. Wilson and M. P. Allen, Mol. Cryst. Liq. Cryst. **198**, 465 (1991).
[18] C. McBride, M. R. Wilson, and J. A. K. Howard, Mol. Phys. **93**, 955 (1998).
[19] D. L. Cheung, S. J. Clark, and M. R. Wilson, Chem. Phys. Lett. **356**, 140 (2002).
[20] M. J. Cook and M. R. Wilson, Mol. Cryst. Liq. Cryst. Sci. Technol., Sect. A **363**, 181 (2001).
[21] M. R. Wilson, J. Chem. Phys. **107**, 8654 (1997).
[22] H. Fukunaga, J. Takimoto, and M. Doi, J. Chem. Phys. **120**, 7792 (2004).
[23] C. McBride and M. R. Wilson, Mol. Phys. **97**, 511 (1999).
[24] C. Zannoni, J. Mater. Chem. **11**, 2637 (2001).
[25] R. Berardi, D. Micheletti, L. Muccioli, M. Ricci, and C. Zannoni, J. Chem. Phys. **121**, 9123 (2004).
[26] A. Lyulin, M. Al-Barwani, M. Allen, M. Wilson, I. Neelov, and N. Allsopp, Macromolecules **31**, 4626 (1998).
[27] P-Y. Lui, N. Yao, and A. M. Jamieson, Macromolecules **32**, 6587 (1999).
[28] P. Martinoty, L. Hillilou, M. Mauzac, L. Benguigui, and D. Collin, Macromolecules **32**, 1746 (1999).
[29] M. R. Wilson, J. Chem. Phys. **107**, 8654 (1997).
[30] A. V. Lyulin, M. S. A. Barwani, M. P. Allen, M. R. Wilson, I. Neelov, and N. K. Allsopp, Macromolecules **31**, 4626 (1998).
[31] M. R. Wilson, J. Chem. Phys. **107**, 8654 (1997).
[32] M. G. Martin and J. I. Siepmann, J. Phys. Chem. B **103**, 4508 (1999).
[33] S. K. Nath and R. Khare, J. Chem. Phys. **115**, 10827 (2001).
[34] J.-P. Ryckaert, Mol. Phys. **55**, 549 (1985).
[35] E. de Miguel, L. F. Rull, M. K. Chalam, and K. E. Gubbins, Mol. Phys. **74**, 405 (1991).

[36] E. de Miguel, E. M. del Rio, J. T. Brown, and M. P. Allen, J. Chem. Phys. **105**, 4234 (1996).
[37] J. T. Brown, M. P. Allen, E. M. del Rio, and E. de Miguel, Phys. Rev. E **57**, 6685 (1998).
[38] M. P. Allen and D. J. Tildesley, *Computer Simulation of Liquids* (Oxford University Press, Oxford, 1987), Chap. 3.
[39] G. R. Luckhurst and G. Saielli, J. Chem. Phys. **112**, 4342 (2000).
[40] L. M. Blinov, in *Handbook of Liquid Crystals*, edited by D. Demus, J. Goodby, G. W. Gray, H.-W. Spiess, and V. Vill (Wiley, Weinheim, 1998), Vol. 1, Chap. 9.
[41] M. R. Wilson, *Physical Properties of Liquid Crystal Nematics* (Institute of Electrical Engineers, London, 2001), Chap. 12, pp. 611–652.
[42] A. Al Sunaidi, W. K. Den Otter, and J. H. R. Clarke, Philos. Trans. R. Soc. London, Ser. A **362**, 1773 (2004).
[43] S. T. Cui, P. T. Cummings, and H. D. Cochran, Fluid Phase Equilib. **141**, 45 (1997).
[44] J.-P. Ryckaert and A. Bellemans, Faraday Discuss. Chem. Soc. **66**, 95 (1978).
[45] D. J. Cleaver, C. M. Care, M. P. Allen, and M. P. Neal, Phys. Rev. E **54**, 559 (1996).
[46] N. L. Allinger, J. Am. Chem. Soc. **99**, 8127 (1977).